102000-22-L
24 June 1974

Mapping Exposed Silicate Rock Types and Exposed Ferric
and Ferrous Compounds from a Space Platform

Quarterly Report for Period 8 March - 8 June 1974

EREP Investigation 444M
NASA Contract NAS9-13317

Prepared by

Robert K. Vincent - Principal Investigator

NASA Technical Monitor

Mr. Timothy White/TF6
National Aeronautics and Space Administration
Johnson Space Center
Principal Investigator Management Office
Houston, Texas   77058

Mapping Exposed Silicate Rock Types and Exposed Ferric
and Ferrous Compounds from a Space Platform

Quarterly Report for Period 8 March - 8 June 1974

The following report serves as the fifth quarterly report for this
contract, which is entitled "Mapping Exposed Silicate Rock Types and
Exposed Ferric and Ferrous Compounds from a Space Platform." The financial
reports have been submitted monthly under separate cover.

During this quarter, screening film was received for SL-4 data, start/
stop times of S-192 data were defined for the Southern California test site,
a paper was presented at the Ninth Remote Sensing of Environment Symposium
which theoretically (based on laboratory spectra) predicts the usefulness
of S-192 data for geological remote sensing, and ratio processing of actual
S-192 line-straightened data (received from NASA for another ERIM contract)
was begun for algorithm testing purposes on an area near White Sands, New
Mexico. The screening film of S-192 data over Southern California of bands
6, 9, and 13-1 are encouraging from the standpoint of apparently good
signal-to-noise. The Pisgah Crater test site was only partially covered
by the data collected, but the remainder of the image strip provides enough
geological targets to make up for the uncovered portions of the test area.
The S-192 start and stop times requested for line straightening are as
follows:

START 026:19:42:21 GMT

STOP 026:19:43:25 GMT

The data were collected on 26 January 1974, but the regions of interest are
free of snow and clouds.

The contrast in thermal image (from band 13-1) may be good enough to
enable detection of very warm geothermal areas. An ozalid color composite was
made of the three channels of data to search for areas which have high visible-
reflective IR albedo, but yet are warmer than average for the scene. For
such anomalous areas, the above-average thermal brightness could be caused by
bright-faced slopes toward the solar direction (sun elevation was approximately
45°, since data collection was at mid-day on 26 January), relatively low thermal

inertia materials, or geothermal heat sources. Geothermal sources close enough to the surface to have temperatures elevated enough to appear warm on SKYLAB S-192 images may also be accompanied by relatively bright clays and possibly iron oxides, both of which can be products of hydrothermal alteration. Thus far, two anomalies have been found in the color composite which have high visible-reflective IR albedo and yet are warmer than average. [Note: This is neither a sufficient nor necessary condition for geothermal sources; it only elminates the low albedo-high temperature targets.] One area is small (about 1 km diameter) and occurs about two miles north of a concealed portion of the Pinto Mountain fault, just west of Twenty-Nine Palms, California. From a recent geologic map, there is no evidence of either an appreciable slope or geothermal activity. The other area, for which a geologic map has been ordered, is in the Southern end of Palen Valley. The 1:250,000 topographic map for the Salton Sea region shows that sand dunes and Palen Dry Lake are in the general vicinity of this anomaly, which would suggest that a sunward-facing slope of bright material (such as sand) may be causing the anomaly. These areas will be checked in the field within the next six months, if possible. In addition there are warm places along the San Andreas fault, but not even low albedo could be excluded from the possible causes of the slightly above-average temperatures of those places by this rather crude color composite method.

The paper presented at the Symposium (Ann Arbor, Michigan) in April, entitled "SKYLAB S-192 Ratio Codes of Soil, Mineral, and Rock Spectra for Ratio Image Selection and Interpretation," is reprinted at the end of this quarterly report. It is a limited systems study of the S-192 scanner for geological remote sensing, using 211 laboratory spectra as "signatures" of various rocks, minerals, and soils. Included in it are the following significant items of information:

1) Prioritization of the single channels of SKYLAB for compositional mapping.

2) Selection of twelve (of a possible sixty-six) best ratios for compositional mapping.

3) Ratio codes of the top twelve spectral ratios for all 211 samples, for choosing the best ratio image to enhance particular geologic targets.

4) When to use single channel inputs and when to use ratio inputs for automatic recognition.

5) What geologic classes SKYLAB S-192 data are expected to separate well and poorly.
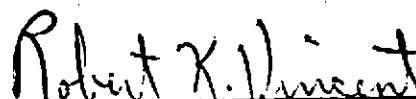
This paper should be helpful to all investigators using ratioing for compositional mapping, and may be of assistance in the selection of spectral channels for future satellites. It is the most significant work reported thus far in this contract.

Finally, it has been decided to use line-straightened S-192 data already supplied to ERIM under another contract (NAS9-13386) for the purpose of testing the ratio algorithms to be used later with Southern California data of SL-4. The in-house data (White Sands, New Mexico) are rather bland in geological content compared with ·the Southern California test site, but it will be used to prepare the way for the SL-4 data, whenever it becomes available. More will be reported on this subject next quarter.

Respectfully submitted:

Robert K. Vincent
Principal Investigator

Approved by:

Richard R. Legault
Director - Infrared and Optics
Division

RKV/RRL/dlc

attachment

SKYLAB S-192 RATIO CODES OF SOIL, MINERAL, AND

ROCK SPECTRA FOR RATIO IMAGE SELECTION AND INTERPRETATION

R. K. Vincent
W. W. Pillars

Environmental Research Institute of Michigan
Ann Arbor, Michigan

ABSTRACT

The SKYLAB S-192 multispectral scanner has twelve channels in the 0.4 - 2.5 μm wavelength region and a single broad-band thermal infrared channel, intended solely for temperature measurements. Since spectral ratio images have been shown with other scanners to be useful for enhancing certain geologic targets and for suppressing unwanted atmospheric and solar illuminations across the scanned scene, ratioing will be employed for similar purposes with SKYLAB data. There are 66 spectral ratios (excluding reciprocals) that can be constructed from the twelve visible-reflective infrared channels of the S-192 scanner. Clearly, it is not economically feasible to produce all possible ratio images for large blocks of SKYLAB data. To aid investigators in selecting optimum ratio images, all possible SKYLAB single channel reflectances and ratios were calculated for approximately 211 laboratory spectra of soils, minerals, and rocks. Linear discriminant analysis was used to separately rank the twelve SKYLAB channels and sixty-six ratios according to their ability to classify these laboratory samples into seventeen assigned classes. The twelve highest ranked ratios were converted to ratio codes, which compress each spectrum in the 0.4 - 2.5 μm wavelength region to a single number. The ratio codes can be used to select the ratio images which will best enhance a target of interest. They can also be easily searched for false alarm candidates (or "look-alikes") of a given target.

For automatic geologic mapping, twelve single channel inputs to linear discriminate analysis were found superior for seven geologic classes, twelve ratio inputs to the same statistical analysis were superior for six classes, and the two cases produced nearly equivalent results for four classes. However, the greater independence of ratios on environmental and instrumental noise tends to favor ratios for the latter four classes. Because of their simplicity and photo-interpretability, ratio images are recommended over automatic mapping methods for those materials which the ratio codes indicate can be enhanced by ratioing.

The results of this study indicate that the SKYLAB S-192 scanner should be most useful for mapping products of hydrothermal alteration, weathering, and evaporation, but that discrimination among igneous rocks will be difficult. This suggests that S-192 data should be quite useful for mineral exploration, but the full potential of general surface geologic mapping by satellite will probably not be reached until high spatial resolution (<30m) scanners with multiple-channel thermal infrared capability have been orbited.

INTRODUCTION

The first ratio image from multispectral scanner data was produced in 1970 from aircraft data and reported in the Seventh International Symposium on Remote Sensing of Environment [1]. In that experiment, the radiances of two thermal infrared channels were ratioed, resulting in a ratio image which was crudely correlated with SiC_2 content of exposed rocks. Since then, spectral ratio imaging has been employed by several investigators of various disciplines. Some of the most recent geological applications of ratio imaging have been for the purpose of enhancing iron oxides in ERTS MSS data [2,3]. Plans are now being made by many geological investigators to utilize the SKYLAB S-192 multispectral scanner for geological remote sensing. They will be attempting to enhance particular minerals and rocks and to perform general geological mapping. Some of this processing will involve spectral ratioing. A typical number of single channels or ratios utilized for producing automatic recognition maps is six. However, there are twelve S-192 channels in the 0.4 - 2.5 μm spectral region, from which sixty-six unique (non-reciprocal) spectral ratios can be formed. There is a clear need to prioritize both the single channels and ratios according to their ability to discriminate among rocks, minerals, and soils for geological remote sensing experiments from SKYLAB S-192 data.

The purpose of this paper is to provide qualified answers to the following questions concerning the twelve visible-reflective IR channels of the SKYLAB S-192 scanner, on the basis of 211 laboratory spectra of rocks, minerals, soils, and some vegetation:

1) What are the best single channels with which to produce automatic recognition maps for geological remote sensing?

2) What are the best spectral ratios with which to produce automatic recognition maps for geological remote sensing?

3) What materials can be enhanced in a single spectral ratio image, and which ratio should be chosen for each of these materials?

4) For which classes of geological targets do single channels provide better multispectral discrimination than spectral ratios, and vice versa?

5) What geologic classes will SKYLAB S-192 be most capable of discriminating?

The qualifications to the answers to these questions will be threefold: no environmental (atmosphere, solar illumination, etc.) or instrumental (electrical noise, gain factors, etc.) effects are considered; the 211 laboratory spectral utilized represent available data and do not provide good statistical samples of all target classes; and the seventeen target classes defined for this study are somewhat subjective.

METHODOLOGY

The Earth Resources Spectral Information System (ERSIS), created for NASA by ERIM, contains over 3,000 reflectance spectra of natural materials [4,5,6]. ERSIS was searched for all spectra of rocks, minerals, and soils that spanned the 0.4 - 2.5 μm wavelength region and which represented the more realistic grain-sized samples (samples with particle diameters exclusively less then 74 μm were omitted). To this, three vegetation spectra (coarse grass, clover, and dead grass) were added. The resulting 211 spectra, which hereafter will be called the geological data collection, were divided into seventeen classes, as shown by Table 1. The mineral classes, 1-9 and 17, represent spectra of pure minerals.

Linear discriminant analysis [7] was the method selected for prioritizing the S-192 channels and spectral ratios according to their ability to discriminate among the seventeen classes of Table 1. This method, which assumes equal covariances, is not expected to be as powerful as the STEP-L program [8] of ERIM, which chooses best channels by minimizing the average pairwise probability of misclassification, but the linear discriminant analysis method is currently more amenable to the use of laboratory spectra as signatures. Given the known reflectance spectra of seventeen classes of materials, an unidentified reflectance spectrum can be classified as one of these classes by calculating its discriminant function for each of the seventeen classes, and assigning the unknown spectrum to the class for which it had the largest discriminant function. The equation for the discriminant function D_{ik} of the ith target class for the kth sample spectrum in the ith target class is given by

$$D_{ik} = a_{io} + \sum_{j=1}^{n} a_{ij} \, c_{jik} \tag{1}$$

where

c_{jik} = spectral parameter of the kth sample spectrum of the ith class for the jth channel (or jth ratio)

n = number of channels (or ratios)

a_{io} = constant for the ith class

a_{ij} = discriminant coefficient for the ith class and jth channel (or ratio)

When only single channels are used as inputs to this classification scheme, c_{jik} is the average laboratory-measured reflectance of the i, kth sample in the spectral region covered by the jth multispectral scanner channel. When spectral ratios are the only inputs, c_{jik} is the quotient resulting from a division of laboratory-measured reflectances in the two wavelength regions covered by the two multispectral scanner channels used to form the jth ratio. There is only one set of coefficients (a_{io} and a_{ij}'s) for each target class. When an unknown geological sample is to be classified, its

TABLE 1

ROCK, MINERAL, SOIL, AND VEGETATION CLASSES

CLASS NUMBER (1)	NAME	NUMBER IN CLASS (K_1)
1	Oxides and hydroxides (Excluding Common Iron Oxides)	27
2	Sulfur, Sulfides, and Sulfates	24
3	Halides	6
4	Phosphates	5
5	Carbonates	29
6	Clay Minerals	8
7	Quartz and Feldspars	19
8	Ferromagnesian Minerals	35
9	Minor Silicate Minerals	8
10	Felsic Rocks and Chert	7
11	Intermediate Rocks	5
12	Basic and Ultrabasic Rocks	9
13	Clay Soils	3
14	Loam Soils	13
15	Sandy Soils and Sand	6
16	Vegetation	3
17	Common Iron Oxides	4

reflectance spectrum is measured, C_{jik}'s are calculated ($C_{jik} = C_{jk}$ for the unknown sample), and substituted into equation (1) for each target class. Hence, for 17 target classes there are seventeen discriminant functions which are calculated. The sample is then classified as belonging to that target class for which the discriminant function is greatest. Geometrically, a discriminant function for a given class describes where the unknown sample spectrum vector lies in n-space, relative to a hyperplane that separates the volume which encloses the given class from the volumes defining each of the other classes.

Although linear discriminant analysis was originally devised as a classification method, it can also be useful for selecting the best channels or ratios for discriminating among the defined target classes (17 in this case). [Note: The method and results described here for ranking single channels and ratios are somewhat different (and better) than those given in the oral presentation of this paper. The following describes the subroutine SEPARATE in the University of Michigan's Statistical Research Laboratory's MIDAS program collection.] The best single channel (or ratio) is chosen on the basis of the largest F-statistic, where

$$F_j = \frac{\dfrac{1}{I-1} \displaystyle\sum_{i=1}^{I} K_i (\overline{X}_{ij} - \overline{X}_j)^2}{\dfrac{1}{(N-I)} \displaystyle\sum_{i=1}^{I} \sum_{k=1}^{K_i} (X_{ijk} - \overline{X}_{ij})^2} \tag{2}$$

where

F_j = F-statistic for jth single channel (or ratio)

I = no. of target classes (17)

K_i = no. of samples in ith target class

N = total no. of samples (211) in the geological data collection

X_{ijk} = observed reflectance (or ratio value) in the jth channel (or ratio) of the kth sample in the ith class

$\overline{X}_{ij} = \dfrac{1}{K_i} \displaystyle\sum_{k=1}^{K_i}$ X_{ijk} = ave. observed reflectance (or ratio value) of the jth channel (or ratio) over the ith class

$\overline{X}_j = \dfrac{1}{N} \displaystyle\sum_{i=1}^{I} \sum_{k=1}^{K_i}$ X_{ijk} = ave. observed reflectance (or ratio value) of the jth channel (or ratio) over all samples in the geological data collection

Once the best channel (or ratio) is chosen, a discriminant function $D_{ikj'}$ is calculated from equation 1 for each sample in the geological data collection, using the best channel (or ratio) and one of the remaining channels (or ratios) denoted by j'. These $D_{ikj'}$ are substituted for the observed reflectances (or ratios), X_{ikj}, in equation 2 and $F_{j'}$ is calculated. For all the other remaining j' channels, $F_{j'}$ are calculated in like manner. The remaining channel with the highest $F_{j'}$ is chosen as second best. This procedure is reiterated, calculating $D_{ikj'}$'s with the best two channels and one of the other remaining channels. The best linear combination of channels (or ratios) is found through this regression procedure. After each new channel is selected, the significance of all channels are tested. If a previously chosen channel becomes less significant than a user-specified level, it is discarded and becomes a member of the "remaining" channels once again. The regression proceeds until a user-specified significance level of the final F-statistic is reached. In this paper, a new channel was selected only if it had a significance level less than 0.10, and a previously chosen channel was rejected if its significance level rose above 0.20.

RANKINGS OF S-192 SINGLE CHANNELS AND SPECTRAL RATIOS

The twelve single channels of the S-192 multispectral scanner were priortized according to the above procedure, with the resulting rankings shown in Table 2. To do this, the average reflectances of all 211 spectra were calculated for the twelve visible-reflective IR S-192 channels, and these average reflectances were substituted into equation 1 as $C_{i,j}$. As an aid to physically understanding the meaning of these rankings, Figure 1 shows the reflectance spectra of a few minerals in the 0.4 - 2.5 µm spectral region. Spectral regions covered by SKYLAB S-192 channels (channels 1-7 are not shown individually) and ERTS MSS channels are shown. The highest ranked channel (2.10 - 2.34 µm) monitors the spectral region in which reflectance minima caused by carbonate (CO_2) and hydroxyl (OH^{-1}) ions occur. The second-ranked channel covers the 0.93 - 1.05 µm spectral region which, according to Figure 1, is primarily monitoring the absorption bands (reflectance minima) produced by transition metal ions (primarily Fe^{2+}, Fe^{3+}, and Cu^{2+}). It is not surprising that the lowest ranked channel covers the 0.42 - 0.45 µm region, because the spectra in Figure 1 show the least spectral contrast from one another in this violet region and not much new information can be obtained from this channel that is not already available from the third ranked channel. It is significant for multispectral scanners that three of the four top-ranked channels are either beyond or on the extreme edge of the spectral range of photographic film.

To find best ratios, all sixty-six non-reciprocal spectral ratios were calculated for the 211 sample spectra, and these were substituted as $C_{i,j}$ into equation 1. Resulting from the same procedure described above, the twelve highest ranked spectral ratios are shown in Table 3. Seven of the top twelve are ratios of adjacent or once-removed channels. Since ratios are a form of non-linear processing, it is not surprising that the highest ranked ratios involve some of the lower ranked single channels. It is significant that the top twelve spectral ratios utilize only ten of the twelve single channels. Channels 1 and 6 were excluded from use in the twelve highest ranked spectral ratios.
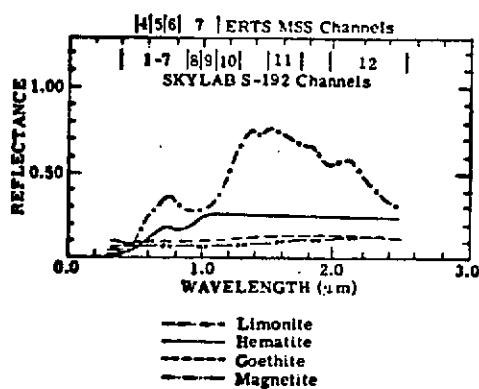
SKYLAB S-192 RATIO CODES

The previous section answered the first two questions posed in the Introduction. The third question will now be addressed: what materials can be enhanced in a single spectral ratio image, and which ratio should be chosen for each of these materials? Because this question requires the reader to examine spectral information from practically all of the 211 spectra in the geological data collection, a form of data compression was instituted. All twelve of the ratios shown in Table 2 were calculated for each of the 211 spectra. For each spectral ratio, a histogram of number of spectra versus ratio value was plotted. From this, ratio ranges were defined such that the spectral curve "population" was divided into deciles, and the ratio range corresponding to the first decile (the 10% of spectral curves with the lowest ratio values) was coded with "0", the second decile with "1", etc., on up to the decile with the highest ratio values, which was coded with "9". The resulting information was used to form a twelve-digit ratio code for each spectral curve, with each digit position describing a different ratio (the highest to lowest ranked ratios go from left-to-right in the ratio code). Table 4 gives the ratio ranges associated with each decile and Table 5 lists the twelve-digit ratio codes for all 211 spectral curves in the geological data collection. The ratios in Tables 4 and 5 correspond to the twelve ratios in Table 3.

Figure 2 gives an example of how to interpret ratio codes. Hematite has a "9" in the third digit position, which means that in an $R_{8,4}$ ratio image (channel 8 divided channel 4 for the S-192 scanner), hematite would appear brighter than 90% of the samples represented by the 211 spectra in the geological data collection. A "0" in the second digit position indicates that in a ratio image of $R_{3,2}$ hematite would appear darker than 90% of the other samples.
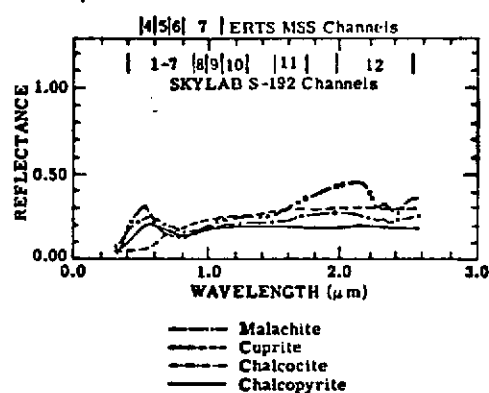
If the assumption could be made that the population of the geological data collection represents well the relative amounts of each target class present in a typical scene, then the phrase "of the other samples represented by the 211 spectra in the geological data bank" could be replaced by "of the materials in the scene". The geological data bank population described in Table 1 probably does not resemble any geological scene closely, but there appear to be enough similarities with arid, and semi-arid terrain to make a loose interpretation of this type useful. Mindful that this gross assumption has been made, for arid and semi-arid terrain it is possible to get an idea of the relative brightness of a given material in each of twelve ratio images by examining the twelve-digit ratio code of that material. The definition of enhancement for the case of ratio images is taken here to mean that a ratio image can be produced in which the target of interest is one of the brightest or darkest objects in the scene. Therefore, those ratios for which a material has a "9" or "0" ratio code are recommended for enhancing that material. In the case of hematite, for example, the $R_{8,4}$, $R_{7,5}$, $R_{8,5}$, $R_{8,7}$, and $R_{3,2}$ ratios would be recommended. Approximately 35% of the 211 samples in the geological data bank have neither a "9" nor "0" in their twelve-digit ratio codes, however. For these materials, ratio image enhancement is less useful. However, the ratio codes should be helpful in interpreting individual ratio images in general, even for those materials not enhanced in the ratio image of interest. For instance, the ratio codes can be easily searched for false alarm
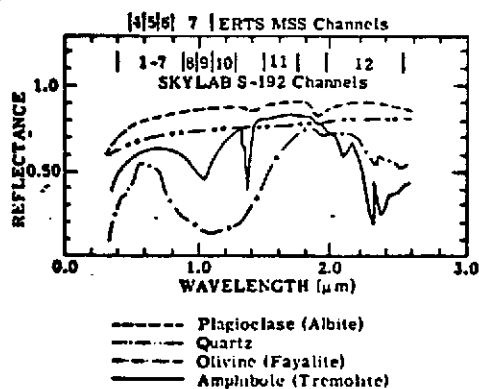
FIGURE 1

SPECTRAL REFLECTANCE OF IRON OXIDES, ORE MINERALS, AND SILICATE MINERALS
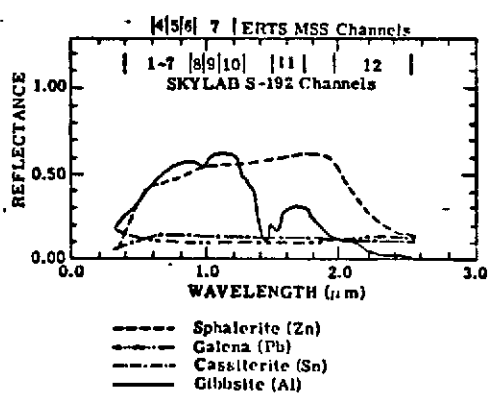ERTS and SKYLAB Multispectral Scanner Channels are indicated on each graph

IRON OXIDES

ERTS MSS Channels |4|5|6| 7
SKYLAB S-192 Channels | 1-7 |8|9|10| |11| | 12

- - - Limonite
——— Hematite
- - - Goethite
— - — Magnetite

COPPER ORE MINERALS

ERTS MSS Channels |4|5|6| 7
SKYLAB S-192 Channels | 1-7 |8|9|10| |11| | 12

- - - Malachite
- - - Cuprite
- - - Chalcocite
——— Chalcopyrite

EXAMPLES OF SILICATE MINERALS

ERTS MSS Channels |4|5|6| 7
SKYLAB S-192 Channels | 1-7 |8|9|10| |11| | 12

- - - Plagioclase (Albite)
- - - Quartz
- - - Olivine (Fayalite)
——— Amphibole (Tremolite)

LEAD, ZINC, TIN, AND ALUMINUM ORE MINERALS

ERTS MSS Channels |4|5|6| 7
SKYLAB S-192 Channels | 1-7 |8|9|10| |11| | 12

- - - Sphalerite (Zn)
- - - Galena (Pb)
- - - Cassiterite (Sn)
——— Gibbsite (Al)

6

FIGURE 2

TWELVE-DIGIT SKYLAB S-192 RATIO CODE FOR HEMATITE

	$R_{7,5}$	$R_{8,4}$	$R_{12,1}$	$R_{4,2}$	$R_{7,2}$	$R_{8,5}$
	↑	↑	↑	↑	↑	↑
Hematite (74 – 250 μm, Minn.)	9 0	9 1	6 8	5 8	8 8	9 9
	↓	↓	↓	↓	↓	↓
	$R_{3,2}$	$R_{10,9}$	$R_{7,3}$	$R_{4,3}$	$R_{7,4}$	$R_{8,7}$

where $R_{i,j} = \dfrac{\rho_i}{\rho_j}$

and ρ_i and ρ_j are the integrated reflectances of a laboratory spectrum of hematite in the ith and jth spectral channels of the SKYLAB S-192 multispectral scanner, respectively.

Each digit corresponds to a ratio range that defines a decile of the population in the data bank. For instance, a 9 in $R_{8,4}$ means that hematite would be brighter in an $R_{8,4}$ ratio image than 90% of the other materials in the data bank.

TABLE 2

RANKING OF SKYLAB S-192 CHANNELS FOR PRODUCING AUTOMATIC RECOGNITION MAPS OF ROCK, MINERAL, AND SOIL CLASSES (BASED ON DISCRIMINANT ANALYSIS OF 211 LABORATORY SPECTRA)

RANK	CHANNEL	
	NUMBER	WAVELENGTH (μm)
1	12	2.10 - 2.34
2	8	0.93 - 1.05
3	2	0.45 - 0.50
4	11	1.55 - 1.73
5	5	0.60 - 0.65
6	4	0.54 - 0.60
7	7	0.77 - 0.89
8	9	1.03 - 1.19
9	10	1.15 - 1.28
10	6	0.65 - 0.73
11	3	0.50 - 0.55
12	1	0.42 - 0.45

TABLE 3

TWELVE BEST RATIOS FOR PRODUCING AUTOMATIC RECOGNITION MAPS
OF ROCK, MINERAL, AND SOIL CLASSES FROM SKYLAB S-192 SCANNER DATA
(BASED ON DISCRIMINANT ANALYSIS OF 211 LABORATORY SPECTRA)

RANK	RATIO	
1	$R_{7,5}$	$= \dfrac{L_7 \ (0.77 - 0.89 \ \mu m)}{L_5 \ (0.60 - 0.65 \ \mu m)}$
2	$R_{3,2}$	$= \dfrac{L_3 \ (0.50 - 0.55 \ \mu m)}{L_2 \ (0.45 - 0.50 \ \mu m)}$
3	$R_{8,4}$	$= \dfrac{L_8 \ (0.93 - 1.05 \ \mu m)}{L_4 \ (0.54 - 0.60 \ \mu m)}$
4	$R_{10,9}$	$= \dfrac{L_{10} \ (1.15 - 1.28 \ \mu m)}{L_9 \ (1.03 - 1.19 \ \mu m)}$
5	$R_{12,11}$	$= \dfrac{L_{12} \ (2.10 - 2.34 \ \mu m)}{L_{11} \ (1.55 - 1.73 \ \mu m)}$
6	$R_{7,3}$	$= \dfrac{L_7 \ (0.77 - 0.89 \ \mu m)}{L_3 \ (0.50 - 0.55 \ \mu m)}$
7	$R_{4,2}$	$= \dfrac{L_4 \ (0.54 - 0.60 \ \mu m)}{L_2 \ (0.45 - 0.50 \ \mu m)}$
8	$R_{4,3}$	$= \dfrac{L_4 \ (0.54 - 0.60 \ \mu m)}{L_3 \ (0.50 - 0.55 \ \mu m)}$
9	$R_{7,2}$	$= \dfrac{L_7 \ (0.77 - 0.89 \ \mu m)}{L_2 \ (0.45 - 0.50 \ \mu m)}$
10	$R_{7,4}$	$= \dfrac{L_7 \ (0.77 - 0.89 \ \mu m)}{L_4 \ (0.54 - 0.60 \ \mu m)}$
11	$R_{8,5}$	$= \dfrac{L_8 \ (0.93 - 1.05 \ \mu m)}{L_5 \ (0.50 - 0.55 \ \mu m)}$
12	$R_{8,7}$	$= \dfrac{L_8 \ (0.93 - 1.05 \ \mu m)}{L_7 \ (0.77 - 0.89 \ \mu m)}$

TABLE 4

RATIO RANGES FOR S-192 RATIO CODES

RATIO	CODE									
	0	1	2	3	4	5	6	7	8	9
$R_{7,5}$	0.392	0.940	1.021	1.063	1.080	1.123	1.157	1.229	1.311	1.499	11.086
$R_{3,2}$	0.754	1.011	1.028	1.045	1.066	1.082	1.116	1.155	1.217	1.397	1.943
$R_{8,4}$	0.277	0.839	0.986	1.049	1.110	1.177	1.255	1.419	1.650	2.589	7.085
$R_{10,9}$	0.858	0.972	0.992	1.000	1.008	1.025	1.034	1.051	1.082	1.199	1.453
$R_{12,11}$	0.162	0.524	0.727	0.828	0.891	0.937	0.998	1.040	1.105	1.267	1.955
$R_{7,3}$	0.336	0.876	1.036	1.095	1.166	1.257	1.381	1.528	1.864	2.808	8.485
$R_{4,2}$	0.743	1.035	1.065	1.090	1.116	1.163	1.214	1.310	1.515	1.860	3.742
$R_{4,3}$	0.893	1.003	1.027	1.036	1.050	1.067	1.095	1.147	1.192	1.365	2.507
$R_{7,2}$	0.382	0.949	1.093	1.139	1.227	1.350	1.512	1.768	2.330	3.521	15.684
$R_{7,4}$	0.319	0.854	1.006	1.063	1.106	1.162	1.232	1.360	1.545	2.124	6.215
$R_{8,5}$	0.331	0.884	0.990	1.051	1.090	1.149	1.191	1.301	1.406	1.672	12.638
$R_{8,7}$	0.589	0.922	0.968	0.991	1.003	1.023	1.038	1.067	1.105	1.181	1.840

TABLE 5

S-192 RATIO CODES OF GEOLOGICAL DATA COLLECTION

ERSIS DOCUMENT NO.	SAMPLE DESCRIPTION		RATIO CODE
830000001	ATACAMITE, NATURAL SURFACE		281191 734135
830000002	SYLVITE	250-1200 MICR	424005 454432
830000003	SYLVITE	74-250 MICR	212004 133410
830000004	ANNABERGITE	74-250 MICR	445021 001268
830000005	ANNABERGITE	250-1200 MICR	153021 561159
830000006	CARNOTITE		797127 978677
830000007	VIVIANITE	74-250 MICR	394196 887445
830000008	VIVIANITE	250-1200 MICR	686697 877652
830000009	COLEMANITE	74-250 MICR	534004 234442
830000010	COLEMANITE	250-1200 MICR	332003 343321
830000011	ULEXITE	74-250 MICR	212002 122222
830010001	GYPSUM DUNE SAND		453002 303332
830010002	PLAYA CRUST		887627 887787
830010003	BASALT, MALPAIS FLOW		747776 456788
800830001	CLAY, GUIBDO GRAVELLY	DRY	678328 888663
800830017	LOAM, CLARION	DRY	979878 778999
800830021	LOAM, HERRACURA PURE SILT	DRY	697728 999751
800830025	LOAM, AGUAN SILT	DRY	688258 788886
800830029	LOAM, AIKEN CLAY	DRY	898548 999872
800830033	SAND, TEXAS DUNE	DRY	888268 888886
800830037	LOAM, MCAULA LIGHT CLAY	DRY	998649 999384
800830041	LOAM, ZANESVILLE SILT	DRY	797757 988777
800830049	LOAM, COLTS NECK TYPE	DRY	896949 999872
800830053	LOAM, RUSTON SANDY TYPE	DRY	789829 999989
800830151	LOAM, MARLBRO HEAVY CLAY	DRY	998249 999982
800830159	LOAM, GREENVILLE TYPE	DRY	999820 999981
800830163	LOAM, SANTA BARBARA TYPE	DRY	797858 999864
800830179	LIMESTONE, SOFT OFF WHITE	DRY	666956 666565
800830183	LOAM, FLAKELY CLAY TYPE	DRY	989459 939997

TABLE 5 (cont.)

S-192 RATIO CODES OF GEOLOGICAL DATA COLLECTION

ERSIS DOCUMENT NO.	SAMPLE DESCRIPTION			RATIO CODE	
800830191	LOAM, BLACK VOLCANIC SANDY	DRY		988548	888598
800830199	SAND, WINDTHORST TYPE	DRY		988578	899899
800830203	CLAY, ALCASO TYPE	DRY		978068	898897
804804001	CALCIUM CARBONATE, GRANULAR			203252	011234
809000003	AMPH.,TREMOLITE	74-250	MICR	221822	232200
809000004	AMPH.,TREMOLITE	250-1200	MICR	140912	443200
809000007	AMPH.,TREMOLITE	74-250	MICR	131441	321112
809000008	AMPH.,TREMOLITE	250-1200	MICR	131811	221100
809000011	AMPH.,ACTINOLITE	74-250	MICR	471921	513110
809000012	AMPH.,ACTINOLITE	250-1200	MICR	561913	514310
809000015	AMPH.,ACTINOLITE	74-250	MICR	160920	511011
809000016	AMPH.,ACTINOLITE	250-1200	MICR	070910	621001
809000019	AMPH.,HORABLENDE	74-250	MICR	857945	205788
809000020	AMPH.,HORABLENDE	250-1200	MICR	123831	111149
809000023	AMPH.,HORABLENCE	74-250	MICR	141891	331136
809000024	AMPH.,HORABLENCE	250-1200	MICR	333792	212233
809000027	AMPH.,HORNBLENDE	74-250	MICR	626985	334567
809000028	AMPH.,HORNBLENCE	250-1200	MICK	142793	553224
809000031	ANDALUSITE	74-250	MICR	667547	777777
809000032	ANDALUSITE	250-1200	MICK	676656	776667
809000035	ANORTHOCLASE	74-250	MICR	767686	666678
809000036	ANORTHOCLASE	250-1200	MICR	666686	666678
809000039	BERYL	74-250	MICK	021750	230019
809000040	BERYL	250-1200	MICR	031820	220009
809000043	PICTITE	250-1200	MICR	374794	665247
809000045	CHABAZITE	74-250	MICR	545115	455555
809000048	CELLSITE	74-250	MICR	566785	655578
809000050	CELLSITE	250-1200	MICR	655860	410006
809000052	CELLSITE	74-250	MICR	062970	300009
809000055	CANCRITE	74-250	MICR	172783	765124

TABLE 5 (cont.)

S-192 RATIO CODES OF GEOLOGICAL DATA COLLECTION

ERSIS DOCUMENT NO.	SAMPLE DESCRIPTION		RATIO CODE
B09000056	DANBURITE	250-1200 MICR	274685 775346
B09000059	CUMORTIERITE	74-250 MICR	808419 467887
B09000060	CUMORTIERITE	250-1200 MICR	908418 267893
B09000062	KAOLINITE	74-250 MICR	343103 454334
B09000063	KAOLINITE	250-1200 MICR	434104 454433
B09000066	TALC	74-250 MICR	132622 332225
B09000067	TALC	250-1200 MICR	050800 541004
B09000070	KAOLINITE	74-250 MICR	555115 555555
B09000071	KAOLINITE	250-1200 MICR	656205 555664
B09000073	MONTMORILLONITE	74-250 MICR	786508 888761
B09000074	MONTMORILLONITE	250-1200 MICR	796408 988751
B09000077	MONTMORILLONITE	74-250 MICR	426728 992643
B09000078	MONTMORILLONITE	250-1200 MICR	182716 867311
B09000081	MUSCOVITE	74-250 MICR	535634 334456
B09000089	OLIVINE-FORSTERITE	74-250 MICR	342533 443321
B09000090	OLIVINE-FORSTERITE	250-1200 MICR	645516 566631
B09000093	OLIVINE-FAYALITE	74-250 MICR	080850 750000
B09000094	OLIVINE-FAYALITE	250-1200 MICR	080970 760000
B09000102	ORTHOCLASE	74-250 MICR	545345 445554
B09000103	ORTHOCLASE	250-1200 MICR	556335 555665
B09000106	ALBITE	74-250 MICR	514364 133455
B09000107	ALBITE	250-1200 MICR	424263 223344
B09000110	OLIGOCLASE	74-250 MICR	433263 333344
B09000111	OLIGOCLASE	250-1200 MICR	444264 444433
B09000114	ANDESINE	74-250 MICR	565475 555567
B09000115	ANDESINE	250-1200 MICR	475665 776457
B09000118	LABRADORITE	74-250 MICR	233372 333234
B09000119	LABRADORITE	250-1200 MICR	222171 211134
B09000122	BYTOWNITE	74-250 MICR	241171 432123
B09000123	BYTOWNITE	250-1200 MICR	261071 552111

TABLE 5 (cont.)

S-192 RATIO CODES OF GEOLOGICAL DATA COLLECTION

ERSIS DOCUMENT NO.	SAMPLE DESCRIPTION			RATIO CODE	
B09000126	PYRX.,AUGITE	74-250	MICR	061871	541114
B09000127	PYRX.,AUGITE	250-1200	MICR	050880	410013
B09000130	PYRX.,DICPSIDE	74-250	MICR	070990	510000
B09000131	PYRX.,DICPSIDE	250-1200	MICR	070990	540000
B09000134	PYRX.,HEDENBERGITE	74-250	MICR	455694	665446
B09000135	PYRX.,MEDENBERGITE	250-1200	MICR	465396	676643
B09000137	PYRX.,HYPERSTHENE	74-250	MICR	777998	777650
B09000138	PYRX.,HYPERSTHENE	250-1200	MICR	161994	665300
B09000141	PYRX.,BRONZITE	74-250	MICR	080890	870008
B09000142	PYRX.,PRONZITE	250-1200	MICR	080990	881003
B09000145	CUARTZ	250-1200	MICR	323373	122345
B09000146	CUARTZ, MILKY	149-250	MICR	535355	444555
BC9000147	CUARTZ, MILKY	250-420	MICR	556455	445566
BC9000155	SERPENTINE	250-1200	MICR	040620	100011
B09004007	CCARSE GRASS		MICR	999115	885996
B09004008	CLOVER		MICR	999115	985998
B09004009	PINE NEEDLES		MICR	999015	955996
B09004010	LAVA, WEATHERED (FEO STAIN)			654725	555551
B09004011	FUMICE			787357	777776
B09004013	LAVA, UNWEATHERED			623583	002453
B09005003	BRUCITE	74-250	MICR	213303	243333
B09005004	BRUCITE	250-1200	MICR	141402	443211
B09005007	CASSITERITE	250-1200	MICR	827147	357862
B09005008	CASSITERITE	74-250	MICR	454045	565551
BU9005011	CHRYSOBRYL	74-250	MICR	645435	444566
BC9005012	CHRYSOBERYL	250-1200	MICR	666625	656667
BC9005017	CORUNDUM	74-250	MICR	717625	005677
B09005018	CORUNDUM	250-1200	MICR	808716	005788
BC9005019	CUPRITE	74-250	MICR	909669	583999
BC9005020	CUPRITE	250-1200	MICR	909665	668599

TABLE 5 (cont.)

S-192 RATIO CODES OF GEOLOGICAL DATA COLLECTION

ERSIS DOCUMENT NO.	SAMPLE DESCRIPTION			RATIO CODE	
809005024	CIASPCRE	74-250	MICR	868617	657898
809005025	CIASPCRE	250-1200 MICR		868617	667788
809005028	GIBPSITE	74-250	MICR	657106	666676
809005029	GIBESITE	250-1200 MICR		767007	777774
809005032	GCETHITE	74-250	MICR	393787	958521
809005033	GCETHITE	250-1200 MICR		194756	887424
809005036	HEMATITE	74-250	MICR	909168	588899
809005039	ILMENITE	74-250	MICR	727576	345677
809005042	LIMCNITE	250-1200 MICR		897915	959860
809005045	MAGNETITE	74-250	MICR	214294	343436
809005048	MAGNETITE	74-250	MICR	141291	201113
809005050	PSILCMELANE	74-250	MICR	404283	012355
809005051	PSILCMELANE	250-1200 MICR		201581	000136
809005053	PYRCLUSITE	74-250	MICR	456844	555479
809005054	PYRCLUSITE	250-1200 MICR		657836	666688
809005057	PYRCLUSITE	74-250	MICR	848787	667888
809005058	PYRCLUSITE	250-1200 MICR		819788	247899
809005060	RUTILE	74-250	MICR	939279	678998
809005061	RUTILE	250-1200 MICR		959185	779999
809005063	RUTILE	74-250	MICR	969859	778999
809005064	RUTILE	250-1200 MICR		979958	778999
809008003	AZURITE	74-250	MICR	103930	000079
809008004	AZURITE	250-1200 MICR		002930	000069
809008006	CALCITE	74-250	MICR	313232	112334
809008009	CALCITE	250-1200 MICR		313322	112345
809008010	CALCITE	74-250	MICR	313342	112333
809008012	CALCITE	250-1200 MICR		211331	111122
809008013	CELEMITE	74-250	MICR	212342	011223
809008014	CELEMITE	250-1200 MICR		202432	011222
809008019	CELEMITE	74-250	MICR	313433	122233

TABLE 5 (cont.)

S-192 RATIO CODES OF GEOLOGICAL DATA COLLECTION

ERSIS DOCUMENT NO.	SAMPLE DESCRIPTION		RATIO CODE	
809008020	DOLOMITE	250-1200 MICR	312423	122322
809008023	MAGNESITE	250-1200 MICR	424133	233445
809008024	MAGNESITE	74-250 MICR	333323	223344
809008026	MAGNESITE	74-250 MICR	231632	332210
809008027	MAGNESITE	250-1200 MICR	130712	322100
809008030	MALACHITE	74-250 MICR	070630	400009
809008031	MALACHITE	250-1200 MICR	060780	200019
809008033	RHODOCHROSITE	74-250 MICR	404456	135710
809008034	RHODOCHROSITE	250-1200 MICR	304537	056700
809009036	SIDERITE	74-250 MICR	670596	776600
809008037	SIDERITE	250-1200 MICR	675197	777720
809008039	SMITHSONITE	74-250 MICR	020930	110000
809008040	SMITHSONITE	250-1200 MICR	020910	000000
809008041	STRONTIANITE	74-250 MICR	535444	344555
809008042	STRONTIANITE	250-1200 MICR	535434	354555
809008044	WITHERITE	74-250 MICR	423253	233345
809008045	WITHERITE	250-1200 MICR	434444	444445
809009003	ALUNITE	74-250 MICR	656007	666764
809009004	ALUNITE	250-1200 MICR	878008	888873
809009011	BARITE	74-250 MICR	777677	987777
809009012	BARITE	250-1200 MICR	788578	888888
809009015	CELESTITE	74-250 MICR	707365	005776
809009016	CELESTITE	250-1200 MICR	808357	006887
809009027	CINNABAR	74-250 MICR	659559	899987
809009028	CINNABAR	250-1200 MICR	749559	899988
809009042	GYPSUM	74-250 MICR	313013	122352
809009043	GYPSUM	250-1200 MICR	222003	123521
809009046	GYPSUM	74-250 MICR	312002	122222
809009047	GYPSUM	250-1200 MICR	312002	112221
809009050	GYPSUM	74-250 MICR	414013	123443

TABLE 5 (cont.)

S-192 RATIO CODES OF GEOLOGICAL DATA COLLECTION

ERSIS DOCUMENT NO.	SAMPLE DESCRIPTION		RATIO CODE
B09009051	GYPSUM	250-1200 MICR	503003 013442
B09009052	GYPSUM	74-250 MICR	515014 124544
B09009060	JAROSITE		395937 998544
B09009086	REALGAR	74-250 MICR	689469 999587
B09009087	REALGAR	250-1200 MICR	889579 999938
B09009096	SULPHUR	74-250 MICR	786466 646676
B09009097	SULPHUR	250-1200 MICR	797466 857777
B09009098	VOLCANIC SUBLIMATE		061251 521013
B09009101	THENARDITE	74-250 MICR	515364 124555
B09009102	THENARDITE	250-1200 MICR	525354 224555
B09012016	HORNBLENCE DIORITE		222271 121122
B09012017	GRANODIORITE		525285 344553
B09012018	PORPHYRY DIORITE		222142 232221
B09012019	GREY RHYOLITE		514184 234443
B09012020	HORNBLENDE GRANITE		525584 223466
B09012021	PORPHYRY ANDESITE		334174 454432
B09012024	PYTCHNITE GABBRO		212261 001122
B09012025	PORPHYRY FELSITE		445574 454555
B09012026	HORNBLENDE ANDESITE		131262 342211
B09012027	PINK RHYOLITE		656287 776665
B09012028	BASALT		101171 000112
B09012029	BIOTITE GRANITE		646586 566666
B09012030	PERIDOTITE-SERPENTINITE		101141 011111
B14004083	SAND, WHITE		848347 336798
B14004084	LAVA		102492 000213
B14004094	MARBLE		302361 000222
A00261001	GREENSTONE, ALTERED BASALT		150850 311111
A00263001	CHERT		766536 664676
A01697001	BASALT LAVA, ALTERED SURFACE		000261 000100
A02010101	SAND, LIGHT TAN WITH GLASS		999949 665553
A02010201	SAND, LIGHT TAN WITH GLASS		999755 989999
A02012101	SAND, COARSE GREY		873567 777787
A02013101	SAND, GRAY WASHED PIT		776746 777666

candidates (or "look-alikes") of a given target. Eventually, these codes may be useful for logic design and memory storage in near-real-time automatic data processors on board space shuttle or aircraft earth resources systems of the future.

PREDICTED COMPOSITIONAL REMOTE SENSING CAPABILITIES OF THE S-192 SCANNER

The final two questions to be addressed are: for which classes of geological targets are single channels better inputs than spectral ratios (and vice versa) for automatic classification by linear discriminant analysis and how well is the S-192 scanner theoretically predicted to perform for each geologic class? To answer these questions, the Mahalonobis distance, a multivariate measure of separation, was calculated for each pair of classes. The Mahalonobis distance is the square of the difference of the mean vectors of two classes weighted by the pooled variance-covariance matrix. The distance between all possible pairs of classes were calculated, along with an F-statistic and a significance level of that F-statistic which indicates how well each pair of geologic classes can be discriminated. The F-statistic here is a multivariate analog of the univariate F-statistic given in equation 2 and is proportional to the Mahalonobis distance. These statistical parameters were calculated for both single channel inputs (all twelve channels), and ratio inputs (top twelve ratios). Table 6 shows a tabulation of the significance levels for all possible pairs of geologic classes. Since this table would be symmetric about the dashed diagonal line for either single channel inputs or ratio inputs alone, the results for single channel inputs are recorded above the diagonal and for ratio inputs are recorded below the diagonal. The class numbers are the same as those in Table 1. The significance level is the probability that the same Mahalonobis distance could have been calculated from two purely random (and inseparable) geologic classes. Hence, the lower the significance level, the better the S-192 scanner should discriminate between the pair of classes. For example, Table 6 shows that for separating classes 17 (common iron oxides) and 12 (basic and ultrabasic rocks), single channel inputs would produce poor results (significance level of 0.290), whereas ratio inputs would easily discriminate between the two classes (significance level $\leq$ 0.000, indicated by a zero). Thus, ratio inputs should be employed for best automatic discrimination of these two classes by the linear discriminant analysis method. In this manner, Table 6 can answer both of the questions posed above.

In order to summarize the results of Table 6, the following evaluation system was adopted. Significance levels greater than 0.100 (which means that there is greater than a 10% chance that the same distance could have been calculated from two random classes) were interpreted to mean that the pair of classes in question could not be discriminated well. For a given class, the number of other classes which could not be discriminated well from it were counted by simply following along the proper row and column of Table 6 and counting the number of times the significance level was greater than 0.100 for single channel inputs and ratio inputs. If there were no other classes which could not be discriminated from a given class, the ability for the S-192 scanner to discriminate that class from all others was rated E for excellent. If only one or two classes could not be discriminated well from the class of interest, a rating of G for good was assigned. An M for medium was assigned for three to five classes not discriminated well, and a P for poor was assigned when S-192 had difficulty discriminating more than five other classes from the class of interest. Table 7 shows the results of this method of evaluation with each of the seventeen classes for both the case of inputting twelve single channels and the case of inputting twelve spectral ratios as C_{jik}'s in equation 1.

Using this method of evaluation, which is conservative in terms of theoretical S-192 capability (possibly nine poorly discriminated classes would have been a better upper limit for the P = poor category), there are seven geologic classes which would appear to be better discriminated by twelve single channel inputs, six classes better discriminated by twelve ratio inputs, and four classes which are discriminated approximately as well by either case. Among the six classes automatically discriminated best by ratio inputs, the common iron oxides and soils are classes for which ratios have been highly recommended by previous investigators [2,3,9] for mapping purposes. Thus, the results of Table 7 seem to be reasonable in light of past experience.

Perhaps the most prominent feature of Table 7 is the difficulty predicted for mapping igneous rocks (classes 10, 11, and 12) with the S-192 scanner. This would indeed be discouraging for geological remote sensing, were it not for the great amount of compositional information available in several medium-width spectral bands in the 8-14 μm thermal IR region [10]. Although SKYLAB cannot collect multichannel thermal IR data (it has only one broad band thermal channel, which cannot yield significant emissivity data), the hope is that future satellite scanners will include three thermal channels, which will give assistance to geological remote sensing precisely where help is needed most. Table 7 shows, however, that the S-192 scanner should be very useful for mapping products of hydrothermal alteration, weathering, and evaporation.

Several points should be emphasized concerning the above comparisons between single channel and ratio inputs to the linear discriminant analysis equations. First, the twelve ratios utilize only ten S-192 channels of data, so in fact a ten-channel scanner is all that would be required to produce these same ratio results. Had more than twelve ratios been selected for comparison with twelve

TABLE 6

SUMMARY OF SEPARATION DISTANCES* FOR 17 GROUPS OF
ROCK, MINERAL, SOIL, AND VEGETATION CLASSES** USING 12 SINGLE CHANNEL
REFLECTANCES AND 12 BEST RATIOS OF SINGLE CHANNELS

CLASS NUMBER	1	2	3	4	5	6	7	8	9	10	11	12	13	14	15	16	17
1	–	0	0	.005	0	0	0	0	0	.055	.290	.059	.091	0	.512	0	.232
2	0	–	0	0	0	0	0	0	0	.001	0	0	.011	0	0	0	0
3	.004	.472	–	0	0	0	0	0	0	0	.001	0	.004	0	0	0	0
4	0	.007	.074	–	0	.001	0	0	.001	.047	.120	.023	.138	.001	.111	0	.013
5	0	0	.004	0	–	0	.002	0	0	.006	.002	0	0	0	0	0	0
6	0	.038	.276	.007	0	–	0	0	0	0	0	0	.069	.002	.001	0	.003
7	.001	.002	.058	.010	.090	0	–	0	0	.417	.006	0	.006	0	.003	0	0
8	0	0	0	0	0	0	0	–	0	.012	.034	0	.001	0	0	0	.006
9	.010	.016	.014	.004	.001	.007	.073	0	–	.016	.005	0	.013	0	.080	0	.012
10	.099	.149	.081	.041	.215	.005	.997	.002	.575	–	.870	.157	.476	.025	.770	0	.081
11	.037	.091	.189	.018	.868	.001	.998	.034	.159	.994	–	.997	.287	.004	.304	0	.322
12	0	0	.003	0	.608	0	.459	.002	.001	.326	.963	–	.059	0	.050	0	.290
13	.005	.114	.018	.008	0	.354	.006	0	.160	.198	.036	0	–	.825	.706	0	.176
14	0	0	0	0	0	0	0	0	0	0	0	0	0	–	.522	0	.119
15	0	0	0	0	0	0	0	0	0	.002	0	0	.018	0	–	0	.418
16	0	0	0	0	0	0	0	0	0	0	0	0	0	0	0	–	0
17	0	0	0	0	0	0	0	0	0	0	0	0	0	.145	0	0	–

*Distance is the Mahalanobis multivariate measure of separation, $V_i - V_j$, where V_i and V_j are the mean vectors of classes i and j.

**Values tabulated are the significance levels (lower significance level means higher probability of separation) of the observed F statistic; upper half for single channel separations, lower half for ratio separations.

TABLE 7

THEORETICAL COMPARISON OF SINGLE CHANNEL AND RATIO DISCRIMINATION FOR
ROCKS, MINERALS, AND SOILS FROM THE SKYLAB S-192 MULTISPECTRAL
SCANNER, EXCLUDING ENVIRONMENTAL VARIABILITY

SYMBOL	NO. OF CLASSES WITH SIGNIFICANCE LEVEL >0.100
E = EXCELLENT	0
G = GOOD	1-2
M = MEDIUM	3-5
P = POOR	>5

CLASS NAME	CLASS NUMBER	SINGLE CHANNEL DISCRIMINATION	RATIO DISCRIMINATION
OXIDES & HYDROXIDES (EXCLUDING COMMON IRON OXIDES)	1	M	E
SULFUR, SULFIDES, & SULFATES	2	E	M
HALIDES	3	E	M
PHOSPHATES	4	M	E
CARBONATES	5	E	M
CLAY MINERALS	6	E	G
QUARTZ & FELDSPARS	7	G	M
FERROMAGNESIAN MINERALS	8	E	E
MINOR SILICATE MINERALS	9	E	M
FELSIC ROCKS & CHERT	10	M	P
INTERMEDIATE ROCKS	11	P	P
BASIC & ULTRABASIC ROCKS	12	M	M
CLAY SOILS	13	P	M
LOAM SOILS	14	M	G
SANDY SOILS & SAND	15	P	E
VEGETATION	16	E	E
COMMON IRON OXIDES	17	P	G

single channel results, the ratio case probably would have been improved. Second, the effects of environmental, instrumental, and bidirectional reflectance variations have been ignored, although it has been shown that spectral ratios are less affected than single channel radiances by such noise [11]. For this reason, ratios are recommended over single channel inputs for the classes indicated in Table 7 as equally discriminated by both cases. Third, Table 7 shows general results for automatic discrimination via the linear discriminant analysis method (these should also be approximately true for discrimination by the maximum likelihood method). However, the capabilities of individual ratios to enhance certain class members are best assessed from the ratio codes of Table 5. The individual ratio enhancement method involves much simpler and cheaper data processing and provides a continuous gray-toned ratio image that lends itself to photogeologic techniques.

CONCLUSIONS

This has been a limited theoretical systems study of the SKYLAB S-192 multispectral scanner capabilities for geological remote sensing. Laboratory spectra of rocks, minerals, soils, and some vegetation were the sole basis for the study, which excluded environmental and instrumental sources of noise from consideration. The twelve S-192 channels between 0.4 μm and 2.5 μm were ranked according to their discrimination ability among seventeen assigned classes of geological targets. The best twelve of a possible sixty-six non-reciprocal spectral ratios were likewise selected, and a comparison was made between the use of twelve single channels and twelve ratios for automatic classification by the linear discriminant analysis method. Although the results of this study show that there were more classes that could be better discriminated by using twelve single channels than by using twelve top-ranked ratios for automatic classification, those ratios utilized only ten of the available twelve channels of information. Also, the inclusion of real-world environmental and instrumental variations would tend to favor ratios over the single channel as inputs to automatic classification methods. In general, it appears that SKYLAB will be most useful for discriminating minerals deposited by hydrothermal alteration, weathering, and evaporation. Discrimination among igneous silicates appears to be difficult with the S-192 scanner, but future scanners can probably overcome these difficulties with multiple channels in the 8 - 14 μm thermal infrared spectral region.

Because of their relatively simple production and photointerpretability, ratio images are recommended over automatic discrimination methods for those geological targets (indicated by the ratio codes) that can be enhanced by ratio imaging. Ratio codes were created to assist in the selection of ratio images for enhancing individual geologic targets. They can also be easily searched for false alarm candidates (or "look-alikes") of a given target. Eventually, ratio codes may be useful for logic design and memory storage in near-real-time automatic data processors on board space shuttle or aircraft earth resources systems of the future.

The results of this study could no doubt be significantly improved by the addition of considerably more spectral curves of field samples to the geological data collection.

ACKNOWLEDGEMENTS

REFERENCES

1. Vincent, R. K. and F. Thomson, Discrimination of Basic Silicates by Recognition Maps Processed from Aerial Infrared Data, Proceedings of the Seventh International Symposium on Remote Sensing of Environment, pp. 247-252, 1971.

2. Rowan, L. C., Wetlaufer, P. H., Goetz, A. F. H., Jr., Billingsly, F. C., and Stewart, J. H., Discrimination of Rock Types and Detection of Hydrothermally Altered Areas in South-Central Nevada by the Use of Computer-Enhanced ERTS Images, U.S. Geological Survey Professional Paper 883, in press.

3. Vincent, R. K., Spectral Ratio Imaging Methods for Geological Remote Sensing from Aircraft and Satellites, Proceedings of American Society of Photogrammetry Management Utilization of Remote Sensing Data Conference, Sioux Falls, South Dakota, pp. 377-397, October 1973.

4. V. Leeman, D. Earing, R. K. Vincent and S. Ladd, The NASA Earth Resources Spectral Information System: A Data Compilation, The University of Michigan Technical Report 3165-24-T, NASA Contract NAS9-9784, 1971.

REFERENCES (cont.)

5. Leeman, V., The NASA Earth Resources Spectral Information System: A Data Compilation – First Supplement, ERIM Technical Report 31650-156-T, NASA Contract NAS9-9784, 1973.

6. Vincent, R. K., The NASA Earth Resources Spectral Information System: A Data Compilation – Second Supplement, ERIM Technical Report 31650-156-T, NASA Contract NAS9-9784, 1973.

7. Morrison, D. F., Multivariate Statistical Methods, McGraw-Hill, New York, New York, 1967.

8. Malila, W. A., R. B. Crane, and W. Richardson, Discrimination Techniques Employing Both Reflective and Thermal Multispectral Signals, ERIM, Ann Arbor, Michigan, Report NASA-CR-ERIM-31650-75-T, NASA Contract NAS9-9784, pp. 41-43, 1973.

9. Wagner, T. W., R. Dillman, and F. J. Thomson, Remote Identification of Soil Conditions with Ratioed Multispectral Data, Remote Sensing of Earth Resources, Space Institute, University of Tenessee, Tullahoma, Tennessee, Volume II, pp. 703-720, 1973.

10. Vincent, R. K., A Thermal Infrared Ratio Imaging Method for Mapping Compositional Variations Among Silicate Rock Types, Ph.D. Dissertation, Department of Geology and Mineralogy, University of Michigan, Ann Arbor, Michigan, 1973.